Atomic layer deposition of bismuth oxide using $Bi(OCMe_2{}^iPr)_3$ and H_2O

Dustin Z. Austin[a),b)]
Department of Electrical Engineering and Computer Science, Oregon State University, Corvallis, Oregon 97331

Derryl Allman, David Price, and Sallie Hose
ON Semiconductor, Technology Development, Gresham, Oregon 97030

Mark Saly[c)]
SAFC Hitech, Haverhill, Massachusetts 01832

John F. Conley, Jr.[d)]
Department of Electrical Engineering and Computer Science, Oregon State University, Corvallis, Oregon 97331

(Received 18 September 2013; accepted 21 November 2013; published 9 December 2013)

Bismuth oxide thin films were deposited by atomic layer deposition using $Bi(OCMe_2{}^iPr)_3$ and H_2O at deposition temperatures between 90 and 270 °C on Si_3N_4, TaN, and TiN substrates. Films were analyzed using spectroscopic ellipsometry, x-ray diffraction, x-ray reflectivity, high-resolution transmission electron microscopy, and Rutherford backscattering spectrometry. Bi_2O_3 films deposited at 150 °C have a linear growth per cycle of 0.039 nm/cycle, density of 8.3 g/cm^3, band gap of approximately 2.9 eV, low carbon content, and show the β phase structure with a (201) preferred crystal orientation. Deposition temperatures above 210 °C and postdeposition anneals caused uneven volumetric expansion, resulting in a decrease in film density, increased interfacial roughness, and degraded optical properties. © *2014 American Vacuum Society*. [http://dx.doi.org/10.1116/1.4840835]

I. INTRODUCTION

Bismuth oxide (Bi_2O_3) has a number of useful material properties which include a high refractive index of n = 2.5 at 632 nm, optical nonlinearity, a bulk density of 8.9 g/cm^3, and a high dielectric constant of $\kappa = 18$–32.[1–5] As result, Bi_2O_3 has been utilized in many applications such as gas sensors, photovoltaic cells, solid oxide fuel cells, and optics.[6–12] In addition, Bi_2O_3 is known to readily form solid solutions with rare earth metals and has led to mixed metal films gaining interest for applications such as ferroelectrics, phase change memories, superconductors, and high-κ metal–insulator–metal (MIM) capacitors.[13–21] To date, most reports of thin film Bi_2O_3 have involved deposition using RF magnetron sputtering, pulsed laser deposition, or metal organic chemical vapor deposition (MOCVD). Atomic layer deposition (ALD) is a chemical vapor deposition (CVD) technique in which the precursor and oxidizing agent are introduced sequentially into the chamber with separation by inert gas purges. Deposition is based on self-limiting surface reactions, which allows for inherent atomic scale thickness control and excellent nonuniformity over large areas or high aspect ratio structures. A robust ALD process would enhance existing applications of thin film Bi_2O_3 and potentially enable new practical uses. However, ALD of Bi_2O_3 has typically only been incorporated into multicomponent oxide thin films because of the requirement for a catalyst to drive the ALD reaction or very low growth rates of approximately 0.01 nm/cycle.[22–28] Hatanpää *et al.* compared several Bi precursors and concluded that $Bi(OCMe_2{}^iPr)_3$ showed the highest potential for Bi_2O_3 growth due to its low melting point, high volatility, and high thermal stability.[29] Although Hatanpää *et al.* briefly discussed precursor stability and thick film growth, the Bi_2O_3 films were not fully characterized. In this work, the growth per cycle, nonuniformity, crystal structure, density, interfacial roughness, composition, refractive index, and band gap of Bi_2O_3 deposited via ALD using $Bi(OCMe_2{}^iPr)_3$ and H_2O are reported as a function of deposition temperature and postdeposition annealing.

II. EXPERIMENT

Bi_2O_3 thin films were deposited on $Si/SiO_2/Si_3N_4$, $Si/SiO_2/TaN$, and $Si/SiO_2/TiN$ substrates. Prior to ALD, chemical mechanical polishing (CMP) was used on the insulating SiO_2 layer to form planar substrates. ALD of Bi_2O_3 was performed using alternating pulses of $Bi(OCMe_2{}^iPr)_3$ and H_2O in a Picosun SUNALE R-150B shower head reactor. The $Bi(OCMe_2{}^iPr)_3$ metal precursor was synthesized according to the literature procedure of Hatanpää *et al.*[29] $Bi(OCMe_2{}^iPr)_3$ was delivered to the reaction chamber using a Picosolid Booster delivery system. The N_2 flow rate was set to 150 sccm in all source lines and the pressure in the deposition chamber was approximately 1 Torr. Deposition temperatures between 90 and 270 °C, $Bi(OCMe_2{}^iPr)_3$ precursor temperatures between 85 and 110 °C, and $Bi(OCMe_2{}^iPr)_3$ pulse times between 0 and 2 s were investigated. 120 s N_2 purges were used to produce low film nonuniformity. For most depositions, 500 ALD cycles were used to target a thickness of approximately 18 nm. Postdeposition anneals, when

a)Electronic mail: austind@eecs.oregonstate.edu
b)Summer intern at ON Semiconductor, Technology Development, Gresham, Oregon 97030.
c)Now at Silicon Systems Group, Applied Materials, 974 Arques Ave., Sunnyvale, California 94085.
d)Electronic mail: jconley@eecs.oregonstate.edu

performed, were conducted in a tube furnace using a nitrogen ambient of 5 Torr for 30 min.

Thermal gravimetric analysis (TGA) was performed on a TA Instruments Model Q50 system with a temperature ramp rate of 10 °C/min under a nitrogen ambient at atmospheric pressure. Film morphology, density, thickness, and interfacial roughness were investigated via x-ray reflectivity (XRR) and grazing incidence x-ray diffraction (GIXRD), using a Rigaku Ultima IV with Cu Kα radiation ($\lambda = 1.5406$ Å) at a step size of 0.02° in the range of 10° to 90° and performed at room temperature. Microstructure was analyzed via high-resolution transmission electron microscopy (HRTEM) using a FEI Tecnai F20 with 200 KV accelerating voltage. Index of refraction, nonuniformity, and thickness measurements were conducted using a J. A. Woollam Co., Inc. M2000 spectroscopic ellipsometer in the range of 450–1000 nm and fit using a Cauchy model. Elemental oxygen, bismuth, hydrogen, carbon, nitrogen, and silicon content of the Bi_2O_3 films were determined via Rutherford backscattering spectrometry (RBS) using a NEC Pelletron 3SDH. The band gap was measured by transmission and reflection measurements in the range of 200–1100 nm using an Ocean Optics HR4000 spectrometer.

III. RESULTS AND DISCUSSION

A. Structural and thermal properties of $Bi(OCMe_2{}^iPr)_3$

$Bi(OCMe_2{}^iPr)_3$ is an alkoxide that contains three 2,3-dimethyl–2-butoxide ligands bonded to the bismuth metal center through a bridging oxygen atom, as shown in the inset of Fig. 1. The material is a white, low melting solid with sensitivity to air and moisture.[29] From the TGA weight loss curve also shown in Fig. 1, $Bi(OCMe_2{}^iPr)_3$ begins to evaporate near 90 °C and is stable up to 236 °C with less than 1% residue remaining. The TGA curve has a smooth decrease with no ledges or bumps, which is indicative of a good ALD precursor. A precursor temperature of 90 °C was set as the operating point for this research.

B. $Bi(OCMe_2{}^iPr)_3$ pulse time and growth per cycle

Shown in Fig. 2 is a spectroscopic ellipsometry film thickness wafer map of a 2 s $Bi(OCMe_2{}^iPr)_3$ pulse time performed at 150 °C with 0.1 s H_2O pulses and 120 s N_2 purges repeated for 500 cycles. The deposition pattern in this figure

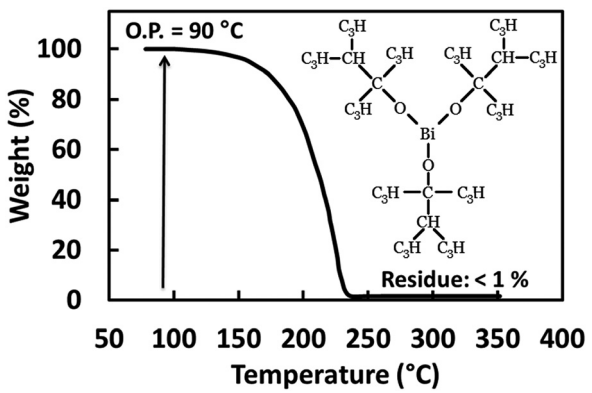

FIG. 1. TGA and molecular structure of $Bi(OCMe_2{}^iPr)_3$.

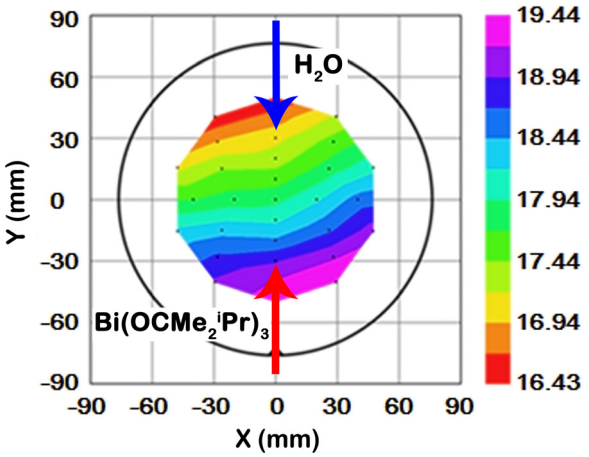

FIG. 2. (Color online) Film thickness wafer map for a 2 s pulse time of $Bi(OCMe_2{}^iPr)_3$ (measured in units of nm).

is produced when $Bi(OCMe_2{}^iPr)_3$ and H_2O are introduced from opposing ports in the reaction chamber. Unless otherwise noted, depositions in the rest of the paper will be performed using the above parameters.

Utilizing the film thickness wafer maps, nonuniformity has been calculated using the standard deviation divided by the average film thickness of all data points measured. In Fig. 3, a plot of film thickness (blue diamonds) and nonuniformity (red squares) as a function of $Bi(OCMe_2{}^iPr)_3$ pulse time is shown. The saturating ALD regime begins at approximately 0.5 s $Bi(OCMe_2{}^iPr)_3$ pulses, with longer pulse times up to 2 s leading to decreased nonuniformity. For a circular area with diameter of 100 mm, the nonuniformity is calculated to be less than 5%.

Using a 2 s $Bi(OCMe_2{}^iPr)_3$ pulse time for best nonuniformity and a Si_3N_4 substrate, a plot of film thickness versus number of cycles is shown in Fig. 4. From the x-axis intercept, there appears to be a nucleation delay of approximately 35 cycles. From the slope, the growth per cycle (GPC) was found to be 0.039 nm/cycle, when film thickness measurements are taken from the center of the wafer. This GPC is consistent with that reported by Hatanpää *et al.* and four times larger than other currently available bismuth precursors such as triphenylbismuth (TPB) and $Bi(thd)_3$, which may help with industrialization of ALD Bi_2O_3.

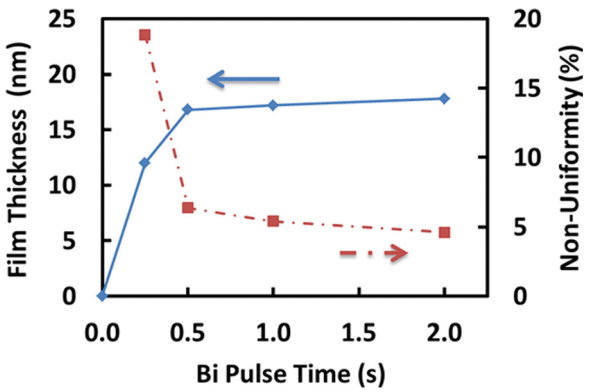

FIG. 3. (Color online) Bi_2O_3 film thickness (blue diamonds) and nonuniformity (red squares) as a function of $Bi(OCMe_2{}^iPr)_3$ pulse time.

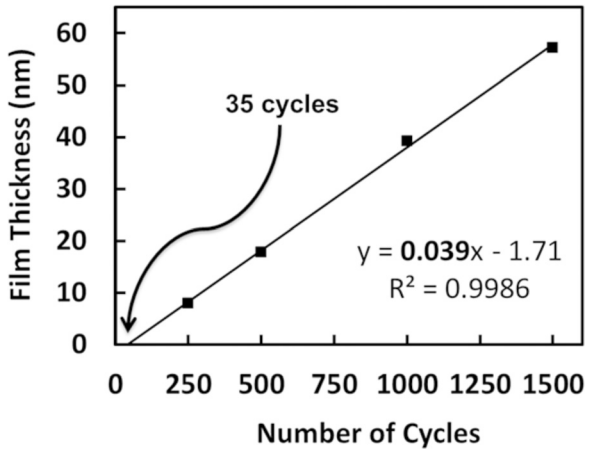

FIG. 4. Bi_2O_3 film thickness vs number of cycles for a 2 s $Bi(OCMe_2{}^iPr)_3$/120 s N_2/0.1 s H_2O/120 s N_2 sequence.

C. Effect of deposition temperature on Bi_2O_3 properties

The crystallographic structure of Bi_2O_3 is known to have a large influence over film properties. Bi_2O_3 forms four crystallographic phases, α, β, γ, and δ, which can be an oxide ionic, p-type, or n-type transparent semiconductor.[30–35] The deposition method as well as the deposition rate can influence whether Bi_2O_3 films are deposited in the monoclinic α phase (fast deposition rate) or the tetragonal β phase (slow deposition rate). Shown in Fig. 5 are GIXRD spectra of Bi_2O_3 films deposited between 90 and 270 °C. Amorphous Si_3N_4 substrates were used in order to obtain a featureless reference scan. ALD is known for fairly slow deposition rates and it is observed that films deposited at 90 °C through 150 °C all show the β phase with a (201) preferred crystal orientation. At a deposition temperature of 210 °C, the film still shows the β phase, but the grains no longer have a single preferred crystal orientation. At 270 °C, the (201) peak has almost completely faded into the background.

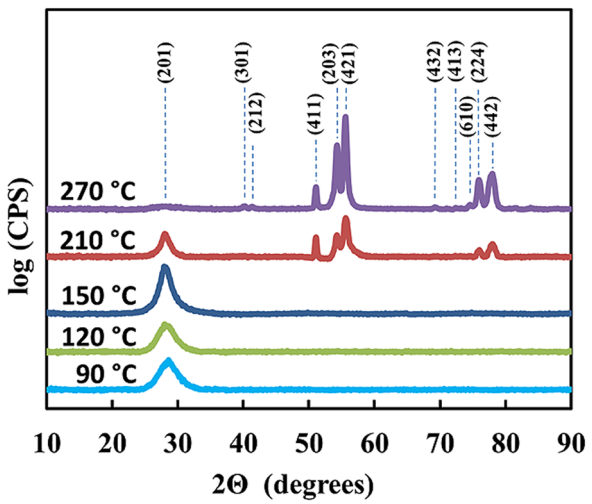

FIG. 5. (Color online) GIXRD spectra of Bi_2O_3 films with deposition temperatures between 90 and 270 °C. Dashed vertical lines indicate various peaks of Bi_2O_3 β phase (PDF: 00-027-0050).

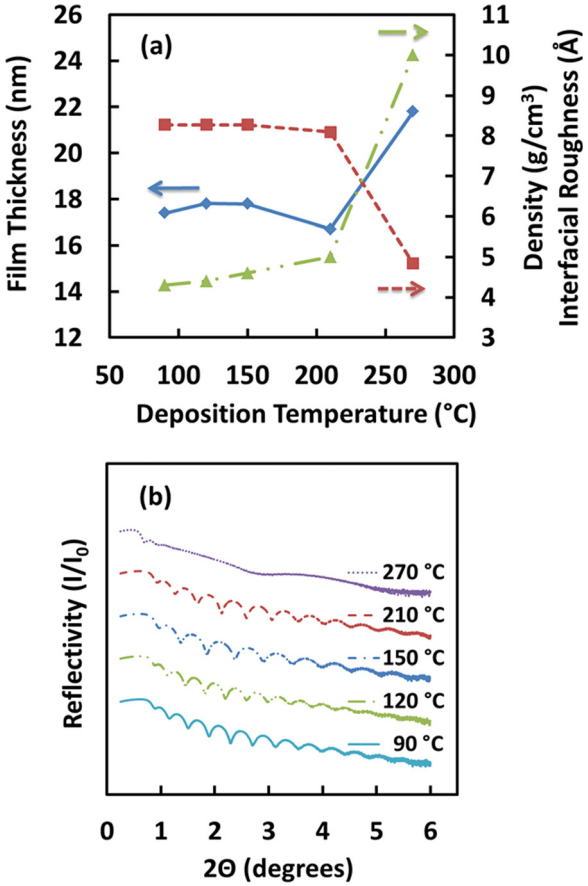

FIG. 6. (Color online) (a) Extracted film thickness (blue diamonds, left axis), density (red squares, right axis), and interfacial roughness (green triangles, right axis) plotted as a function of deposition temperature. (b) XRR spectrum of Bi_2O_3 films with deposition temperatures between 90 and 270 °C.

Further examining the deposition temperature dependence, shown in Fig. 6(a) is a plot of film thickness (blue diamonds), density (red squares), and interfacial roughness (green triangles) obtained from modeling the XRR data in Fig. 6(b). For deposition temperatures up to 210 °C, as deposited films have an interfacial roughness of less than 5 Å, a density of 8.3 g/cm^3 (which is slightly lower than the bulk density of 8.9 g/cm^3), and have an average film thickness ranging between 16.7 and 17.8 nm. Films deposited at

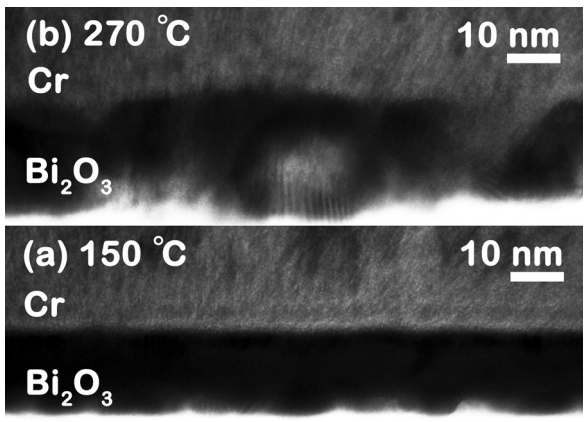

FIG. 7. HRTEM of Bi_2O_3 films deposited at (a) 150 °C and (b) 270 °C.

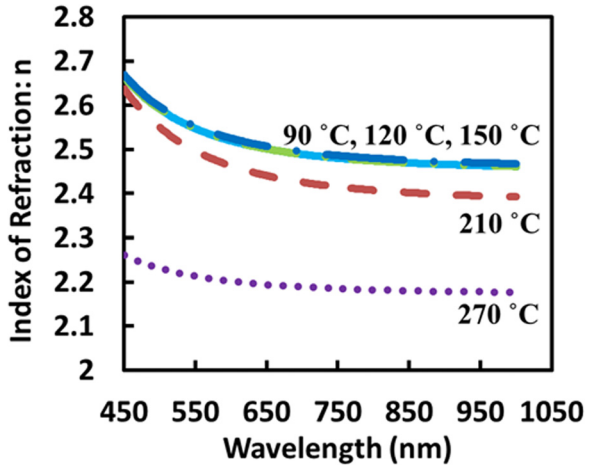

FIG. 8. (Color online) Index of refraction vs wavelength for Bi_2O_3 films with deposition temperatures between 90 and 270 °C.

270 °C show a dramatic increase in both interfacial roughness and average film thickness, which may be explained by the film having enough energy to coalesce into islands as it grows.[36] In addition, density appears to decrease at 270 °C, although it should be noted that due to the accompanying increased roughness in these films, the measurement model accuracy is reduced.

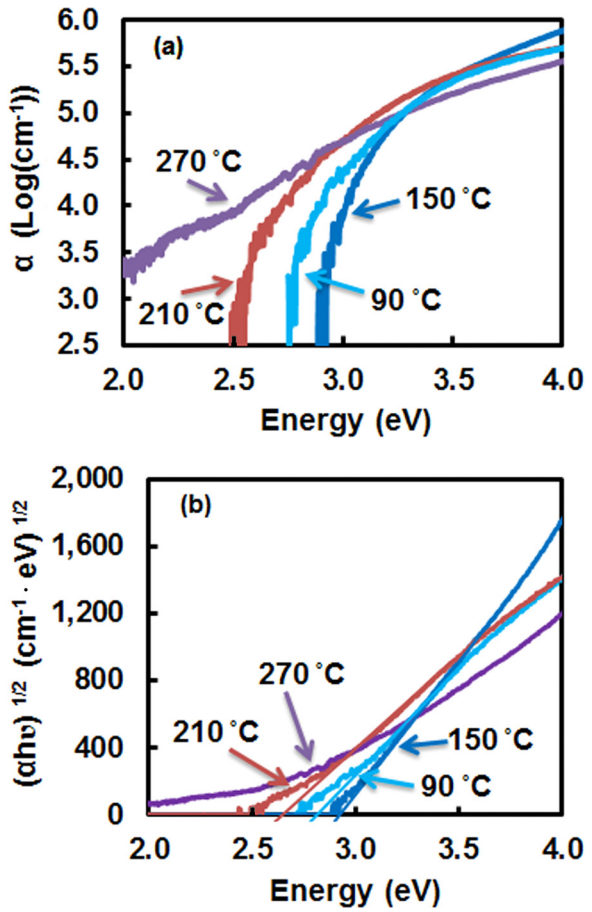

FIG. 9. (Color online) (a) Absorption coefficient (α) vs energy and (b) band gap estimation, $(\alpha h\upsilon)^{1/2}$ vs energy, of Bi_2O_3 films deposited between 90 and 270 °C.

TABLE I. Tabulated values for optical and physical properties of Bi_2O_3 films.

T_{Dep} (°C)	E_g (eV)	n (632 nm)	ε_r (632 nm)	ρ (g/cm^3)
90	2.8	2.50	6.29	8.3
150	2.9	2.51	6.32	8.3
210	2.5	2.45	5.99	8.1
270	—	2.20	4.83	4.8

Due to high thermal expansion coefficients, Bi_2O_3 films are known to show increased volume with increased deposition temperature.[30,31] Shown in Fig. 7 are TEM images of a Bi_2O_3 film deposited at (a) 150 °C and (b) 270 °C. In agreement with the XRR data from Fig. 6, the 150 °C film has low interfacial roughness, while the film deposited at 270 °C has a dramatic increase in both interfacial roughness and average film thickness, consistent with increased volume.

A similar comparison is made characterizing the optical properties for deposition temperatures between 90 and 270 °C. Shown in Fig. 8 are spectra of the index of refraction, n, versus wavelength for the various deposition temperatures. The index of refraction was measured via spectroscopic ellipsometry and is taken as n^2. Shown in Fig. 9(a) is a semi-log plot of absorption coefficient (α) versus energy. The band gap is taken as the energy at which the absorption coefficient abruptly increases.[37] Next in Fig. 9(b) is a plot of $(\alpha h\upsilon)^{1/2}$ versus energy from which the optical band gap may also be estimated by extrapolating the linear portion of each curve to the x-axis. Similar values for the band gap are obtained from both plots, suggesting that the electronic structure has indirect-allowed transitions.[38] The same general trend is observed in which the largest measured band gap is 2.9 eV for a deposition temperature of 150 °C. As deposition temperature increased to 270 °C, the band gap became indeterminable.

The band gap, index of refraction, derived optical dielectric constant, and density for a range of deposition

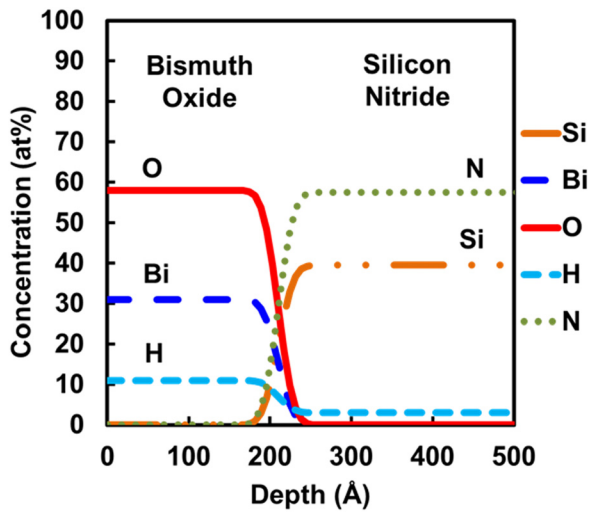

FIG. 10. (Color online) Elemental content obtained from RBS of Bi_2O_3 films deposited at 150 °C.

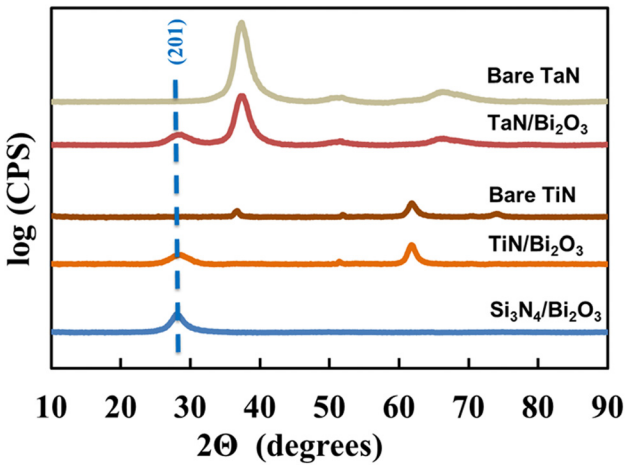

FIG. 11. (Color online) GIXRD spectra of Bi_2O_3 films deposited on Si_3N_4, TaN, and TiN substrates. The dashed vertical line indicate (201) peak of Bi_2O_3 β phase (PDF: 00-027-0050).

temperatures are compiled in Table I. Each parameter indicates the same general dependence on temperature with a maximum at 150 °C. The decrease in these parameters may be explained by the introduction of defect bands as the films become less ordered. As seen previously via GIXRD spectra, there is peak narrowing as the deposition temperature increases to 150 °C but a shift away from a single preferred crystal orientation above 150 °C.

Shown in Fig. 10 is the RBS atomic concentration versus depth profiles for elemental oxygen, bismuth, hydrogen, carbon, nitrogen, and silicon content in a Bi_2O_3 film deposited at 150 °C on a silicon nitride substrate. The elemental bismuth content is deficient at 31 at. % and appears to be replaced by hydrogen, which suggests there could be unreacted sites left on surface after each $Bi(OCMe_2{}^iPr)_3$ pulse. The carbon content is not shown in Fig. 10 as it was below the detectable limit in all films. The RBS data showed roughly consistent composition for deposition temperatures of 90–270 °C.

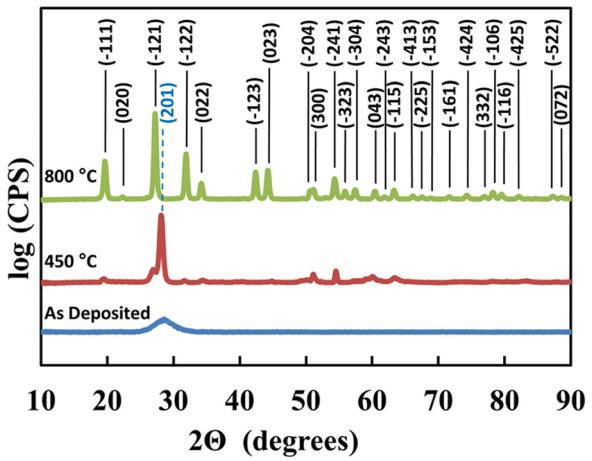

FIG. 12. (Color online) GIXRD spectra of as-deposited and annealed Bi_2O_3 films. Dashed vertical blue line indicates Bi_2O_3 β phase (PDF: 00-027-0050); solid vertical black lines indicate Bi_2O_3 α phase (PDF: 01-071-0465).

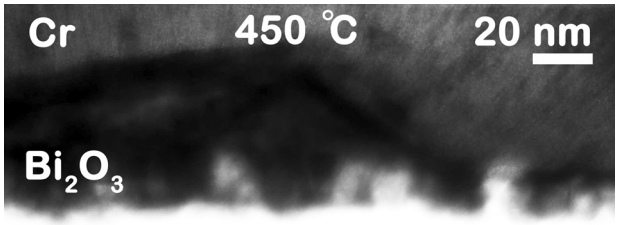

FIG. 13. HRTEM of 450 °C annealed Bi_2O_3.

D. Substrate impact on film morphology

The crystallographic orientation of the substrate is known as a potential source of influence on the morphology of overlying films. In addition to amorphous Si_3N_4, conductive polycrystalline substrates of TaN and TiN are investigated for their influence on the growth of Bi_2O_3 films. TiN and TaN substrates were chosen for their prominent role in back end of line (BEOL) applications in microelectronics. Displayed in Fig. 11 is GIXRD intensity versus 2θ spectra for various substrates with and without overlying ALD Bi_2O_3 films. Bare TaN and TaN/Bi_2O_3 are grouped together at the top, bare TiN and TiN/Bi_2O_3 are grouped in the middle, and the reference silicon nitride/Bi_2O_3 is at the bottom. First focusing on the TaN group at the top, the only difference between the two spectrum is the appearance of the β-phase related (201) peak at $2\theta = 28.6°$ in the Bi_2O_3 coated sample. Next, considering the TiN group in the middle, the results are very similar with the additional (201) peak in the Bi_2O_3 coated sample being the only difference. For all three substrates, only the same (201) peak of the Bi_2O_3 β-phase is observed, indicating that these substrates produce little influence on the overlying Bi_2O_3 film morphology.

E. Impact of annealing

Shown in Fig. 12 are GIXRD spectra of Bi_2O_3 thin films annealed for 30 min at 5 Torr in N_2 at 450 and 800 °C, with measurements made post cooling at 30 °C. The 450 °C spectrum has a strong peak at 28.6° corresponding to the (201) peak of the β phase with weaker peaks from the α phase. The 800 °C spectrum appears to fully transition into the α phase upon cooling. In Fig. 13, a post 450 °C anneal HRTEM image reveals that the Bi_2O_3 film exhibits large uneven volumetric expansion, which is in agreement with literature reports for Bi_2O_3.[30,31] Finally, the 800 °C annealed films were observed to delaminate from the substrate.

IV. SUMMARY AND CONCLUSION

In conclusion, Bi_2O_3 thin films were deposited by ALD using $Bi(OCMe_2{}^iPr)_3$ and H_2O at deposition temperatures between 90 and 270 °C on Si_3N_4, TaN, and TiN substrates. For films deposited at 90–150 °C, the Bi_2O_3 β phase with single preferred crystal orientation of (201) was observed and found to be independent of the underlying substrates. RBS indicates films are carbon free but contain excess hydrogen. Films with deposition temperatures greater than 150 °C and postdeposition annealed resulted in increased interfacial roughness with reduced band gap, density, and

refractive index. Bi_2O_3 films deposited at 150 °C showed the best film properties with a density of 8.3 g/cm^3, a band gap of 2.9 eV, a refractive index of 2.51 at 632 nm, an optical dielectric constant of 6.32, the lowest interfacial roughness, and a GPC of 0.039 nm/cycle. Due to these film properties combined with high GPC and low C content, $Bi(OCMe_2{}^iPr)_3$ appears to be a candidate for ALD of Bi_2O_3 and multicomponent Bi based oxide thin films.

ACKNOWLEDGMENTS

The authors would like to thank graduate students R. Ravichandran (OSU) and S. Smith (OSU) for assistance with optical and XRR measurements, respectively, C. Tasker (Manager OSU cleanroom) for equipment support, T. Mueller (ON Semiconductor) for assistance with TEM imaging, C. Dezelah (Picosun) for technical discussions, ON Semiconductor for financial support, and SAFC Hitech for providing $Bi(OCMe_2{}^iPr)_3$.

[1]V. Dolocan and F. Iova, Phys. Status Solidi A **64**, 755 (1981).
[2]L. Leontie, M. Caraman, A. Visinoiu, and G. I. Rusu, Thin Solid Films **473**, 230 (2005).
[3]V. Dimitrov and S. Sakka, J. Appl. Phys. **79**, 1736 (1996).
[4]H. Frederikse, *CRC Handbook of Chemistry and Physics* (CRC, Boca Raton, 2003).
[5]S. Condurache-Bota, N. Tigau, A. P. Rambu, G. G. Rusu, and G. I. Rusu, Appl. Surf. Sci. **257**, 10545 (2011).
[6]D. Shan, J. Zhang, H.-G. Xue, Y.-C. Zhang, S. Cosnier, and S.-N. Ding, Biosens. Bioelectron. **24**, 3671 (2009).
[7]B. Sirota, J. Reyes-Cuellar, P. Kohli, L. Wang, M. E. McCarroll, and S. M. Aouadi, Thin Solid Films **520**, 6118 (2012).
[8]K. Kobayashi, J. Non-Cryst. Solids **316**, 403 (2003).
[9]H. Weidong, Q. Wei, W. Xiaohong, D. Xianbo, C. Long, and J. Zhaohua, Thin Solid Films **515**, 5362 (2007).
[10]K. L. Chopra and S. R. Das, *Thin Film Solar Cells* (Plenum, New York, 1983).
[11]T. P. Gujar, V. R. Shinde, C. D. Lokhande, and S.-H. Han, Mater. Sci. Eng. B **133**, 177 (2006).
[12]X. Gou, R. Li, G. Wang, Z. Chen, and D. Wexler, Nanotechnology **20**, 495501 (2009).
[13]W. H. Dumbaugh and J. C. Lapp, J. Am. Ceram. Soc. **75**, 2315 (1992).
[14]Y. Zeng and Y. S. Lin, J. Catal. **182**, 30 (1999).
[15]D. Barreca, G. A. Rizzi, and E. Tondello, Thin Solid Films **333**, 35 (1998).
[16]E. M. Dianov, J. Lightware Technol. **31**, 681 (2013).
[17]C. D. Ling, R. L. Withers, S. Schmid, and J. G. Thompson, J. Solid State Chem. **137**, 42 (1998).
[18]K.-H. Cho, C.-H. Choi, Y. H. Jeong, S. Nahm, C.-Y. Kang, S.-J. Yoon, and H.-J. Lee, J. Electrochem. Soc. **155**, G148 (2008).
[19]B. H. Park, B. S. Kang, S. D. Bu, T. W. Noh, J. Lee, and W. Jo, Nature **401**, 682 (1999).
[20]M. Vehkamäki, T. Hatanpää, M. Kemell, M. Ritala, and M. Leskelä, Chem. Mater. **18**, 3883 (2006).
[21]M. Karimi, R. Tu, J. Peng, W. Lennard, G. H. Chapman, and K. L. Kavanagh, Thin Solid Films **515**, 3760 (2007).
[22]Y. D. Shen, Y. W. Li, W. M. Li, J. Z. Zhang, Z. G. Hu, and J. H. Chu, J. Phys. Chem. C **116**, 3449 (2012).
[23]M. Vehkamäki, T. Hatanpää, M. Ritala, and M. Leskelä, J. Mater. Chem. **14**, 3191 (2004).
[24]S. J. A. Moniz, C. S. Blackman, C. J. Carmalt, and G. Hyett, J. Mater. Chem. **20**, 7881 (2010).
[25]M. Mehring, Coord. Chem. Rev. **251**, 974 (2007).
[26]S. W. Kang and S. W. Rhee, Thin Solid Films **468**, 79 (2004).
[27]G. Bandoli, D. Barreca, E. Brescacin, G. A. Rizzi, and E. Tondello, Chem. Vap. Deposition **2**, 238 (1996).
[28]M. Putkonen and L. Niinistö, *Precursor Chemistry of Advanced Materials* (Springer-Verlag, Berlin, 2005), Vol. 9, pp. 125–145.
[29]T. Hatanpää, M. Vehkamäki, M. Ritala, and M. Leskelä, Dalton Trans. **39**, 3219 (2010).
[30]P. Shuk, H.-D. Wiemhöfer, U. Guth, W. Göpel, and M. Greenblatt, Solid State Ionics **89**, 179 (1996).
[31]M. Yashima, D. Ishimura, and K. Ohoyama, J. Am. Ceram. Soc. **88**, 2332 (2005).
[32]H. A. Harwig and A. G. Gerards, J. Solid State Chem. **26**, 265 (1978).
[33]E. Oniyama and P. G. Wahlbeck, J. Phys. Chem. B **102**, 4418 (1998).
[34]D. Risold, B. Hallstedt, L. J. Gauckler, H. L. Lukas, and S. G. Fries, J. Phase Equilib. **16**, 223 (1995).
[35]R. B. Patil, R. K. Puri, and V. Puri, Arch. Phys. Res. **2**, 31 (2011).
[36]R. L. Puurunen and W. Vandervorst, J. Appl. Phys. **96**, 7686 (2004).
[37]Y. Hishikawa, N. Nakamura, S. Tsuda, S. Nakano, Y. Kishi, and Y. Kuwano, Jpn. J. Appl. Phys., Part 1 **30**, 1008 (1991).
[38]S. Adachi, *Optical Properties of Crystalline and Amorphous Semiconductors: Materials and Fundamental Principles*, 1st ed. (Kluwer Academic, Boston, 1999).